

Supporting Information

Co-based MOF heterogeneous catalyst for efficient degradation of organic dye via peroxymonosulfate activation

Wei Xie,^a Yuan Yuan,^a Jia-Jun Wang,^a Shu-Ran Zhang,^a Guang-Juan Xu,^a Nan Jiang,^a Yan-Hong Xu,^{*a} and Zhong-Min Su^{*b}

^a Key Laboratory of Preparation and Applications of Environmental Friendly Materials (Jilin Normal University), Ministry of Education, Changchun 130103, Jilin, PR China

^b Institute of Functional Material Chemistry, Faculty of Chemistry, Northeast Normal University, Changchun 130024, Jilin (P. R. China)

** Corresponding author*

E-mail: xuyh198@163.com; zmsu@nenu.edu.cn

S1. Materials and characterization

All chemical reagents for synthesis were purchased commercially and were used directly without further purification. Powder X-ray diffraction (PXRD) data were obtained on a Rigaku model RINT Ultima III diffractometer by depositing powder on glass substrate, from $2\theta = 3^\circ$ up to 50° with 0.02° increment. The IR spectrum was measured with a Perkin-elmer model FT-IR-frontier infrared spectrometer. Thermogravimetric analysis (TGA) was recorded on a Q5000IR analyser (TA Instruments) with an automated vertical overhead thermobalance heated from room temperature to 800°C with a heating rate of $5^\circ\text{C}/\text{min}$ under nitrogen gas atmosphere. Elemental analyses (C, H and N) were conducted on a Perkin-Elmer 240C elemental analyzer. The UV-vis absorption spectra were carried out using Jasco V-770 spectrometer (JAPAN) spectrophotometer.

S2. Synthesis of JLNU-500

$\text{Co}(\text{NO}_3)_2 \cdot 6\text{H}_2\text{O}$ (0.058 g, 0.2 mmol), 4-(pyridin-4-yl) benzoic acid (HPBA, 0.020 g, 0.1 mmol), and 5-aminoisophthalic acid (H_2AIP , 0.018 g, 0.1 mmol) were dissolved in a 6 mL mixture of N,N-dimethylacetamide (DMA) and H_2O (v/v = 1:1). The clear solution was sealed in a 10 mL Teflon-lined stainless vessel and heated at 110°C for 72 h. The vessel was then cooled slowly down to the room temperature. Purple block crystals of **JLNU-500** were separated in 83% yield based on HPBA ligand. Elemental microanalysis for $\text{C}_{32}\text{H}_{41.5}\text{N}_5\text{O}_{10.75}\text{Co}_2$, calculated (%): C, 48.90; H, 5.32; N, 8.91. Found (%): C, 48.67; H, 5.59; N, 8.52. IR data (KBr cm^{-1}): 3616 (w), 3364 (m), 3269 (m), 2932 (m), 1631 (s), 1592 (s), 1572 (s), 1397 (s), 1265 (m), 1187 (m), 1098 (w), 1016 (m), 960 (m), 895 (w), 783 (s), 756 (m), 679 (w), 592 (w), 488 (w).

S3. Heterogeneous RhB degradation by JLNU-500/PMS

In this study, a model pollutant RhB (rhodamine B) is chosen to evaluate the catalytic performance of Co-based MOF **JLNU-500** for PMS activation. The oxidation degradation experiments were proceeded in 100 mL of RhB aqueous solution (50 mg

L⁻¹) in 250 mL reactor. NaOH (0.1 M) and HCl (0.1 M) were used to adjust the initial pH value. The experiments were carried out at 20 °C under ambient atmospheric condition. Before addition of PMS, the solution including **JLNU-500** catalyst (10 mg) and RhB contaminant was magnetically stirred for 10 min. And then we added PMS (30 mg, 1.0 mM) to the system. After desired intervals, 1.0 mL of the degraded solution was taken with adding 1.0 mL of 6 mM Na₂S₂O₃ aqueous solution to quench the reaction and filtered with a 0.22 -µm filter to separate the supernatant liquid from catalyst for analysis. The RhB concentrations were analyzed by using a UV-visible spectrophotometer at its maximum absorbance wavelength of 554 nm. The influence factors of RhB concentration, catalyst loading, PMS concentration, temperature and pH were carried out to assess the performance of RhB degradation. To test the recyclability of **JLNU-500** catalyst, after degradation each experiment, the **JLNU-500** was collected by centrifugation, washed with water and ethanol and dried at 70 °C for 24 h. Then the same catalyst was used for the next run catalytic degradation experiment.

A general pseudo-first-order reaction was used to estimate the degradation reaction rate as shown below:

$$\ln(C/C_0) = -kt$$

where C₀ and C are the initial concentration and the concentration at various time, respectively, *k* is the first order reaction kinetic constant of RhB removal (min⁻¹).

LC-MS method

The reaction intermediates of RhB were identified using liquid chromatography-mass spectrometry (LC-MS) at 554 nm. Water (mobile phase A with a flow rate of 0.25 mL min⁻¹) and methanol (mobile phase B with a flow rate of 0.75 mL min⁻¹) were used as mobile phases. A fixed volume injection loop was used to inject 10 µl of sample.

S4. Single-crystal X-ray diffraction

The X-ray single crystal diffraction data of **JLNU-500** was collected at 296 K on a Bruker APEXII CCD diffractometer with graphite-monochromated Mo K α radiation

($\lambda = 0.71069 \text{ \AA}$). Absorption corrections were applied using multi-scan technique. The structure was solved by Direct Method and refined by full-matrix least-squares techniques using the SHELXL-2018 program¹ within WINGX software². Non-hydrogen atoms were refined with anisotropic temperature parameters. All the solvent molecules which are highly disordered and not able to be modeled were treated by the SQUEEZE³ routine in PLATON⁴. The detailed crystallographic data and structure refinement parameters for **JLNU-500** (CCDC: 2250236) are summarized in Table S1.

Table S1 Crystal data and structure refinements for **JLNU-500**.

Identification code	JLNU-500
formula	$\text{C}_{32}\text{H}_{41.5}\text{Co}_2\text{N}_5\text{O}_{10.75}$
Formula weight	786.06
Crystal system	Monoclinic
Space group	$P2_1/n$
a (Å)	15.649 (7)
b (Å)	12.876 (6)
c (Å)	17.677 (8)
α (°)	90.000
β (°)	107.059 (8)
γ (°)	90.000
V (Å ³)	3405 (3)
Z	4
$D_{\text{calcd.}}$ [g cm ⁻³]	1.533
$F(000)$	1634
Reflections collected / unique	15277 / 5940
$R(\text{int})$	0.0650
Goodness-of-fit on F^2	1.086
R_1^a [$I > 2\sigma(I)$]	0.0677
wR_2^b (all data)	0.1872

$$^a R_1 = \frac{\sum ||F_o| - |F_c||}{\sum |F_o|}, ^b wR_2 = \frac{|\sum w(|F_o|^2 - |F_c|^2)|}{\sum |w(F_o^2)|^{1/2}}$$

Table S2 Selected bond lengths (Å) for **JLNU-500**.

Atom	Atom	Length/Å	Atom	Atom	Length/Å
Co1	O1#1	2.120(3)	Co2	O2#1	2.033(4)
Co1	O4#2	2.067(3)	Co2	O3	1.980(4)
Co1	O6	2.188(4)	Co2	O5	2.003(4)
Co1	O7	2.046(3)	Co2	O7	2.012(4)
Co1	N1#3	2.209(5)	Co2	O7#2	2.146(3)
Co1	N2#4	2.208(4)			

#1 1/2-X, -1/2+Y, 1/2-Z; #2 1-X, 1-Y, 1-Z; #3 -1/2+X, 1/2-Y, 1/2+Z; #4 1/2+X, 1/2-Y, 1/2+Z.

Table S3 Selected bond angles (°) for **JLNU-500**.

Atom	Atom	Atom	Angle/°	Atom	Atom	Atom	Angle/°
O1#1	Co1	O6	92.61(16)	O7	Co1	N2#3	168.78(16)
O1#1	Co1	N1#2	87.72(17)	N2#3	Co1	N1#2	101.12(18)
O1#1	Co1	N2#3	82.52(15)	O2#1	Co2	O7#4	174.52(17)
O4#4	Co1	O1#1	167.01(13)	O3	Co2	O2#1	86.23(15)
O4#4	Co1	O6	89.90(16)	O3	Co2	O5	107.0(2)
O4#4	Co1	N1#2	89.14(18)	O3	Co2	O7#4	92.38(14)
O4#4	Co1	N2#3	85.73(15)	O3	Co2	O7	141.02(18)
O6	Co1	N1#2	177.10(17)	O5	Co2	O2#1	99.87(18)
O6	Co1	N2#3	76.07(16)	O5	Co2	O7#4	85.60(15)
O7	Co1	O1#1	93.12(14)	O5	Co2	O7	110.89(16)
O7	Co1	O4#4	99.42(14)	O7	Co2	O2#1	96.09(15)
O7	Co1	O6	93.89(15)	O7	Co2	O7#4	81.67(14)
O7	Co1	N1#2	88.97(17)				

#1 1/2-X, -1/2+Y, 1/2-Z; #2 -1/2+X, 1/2-Y, 1/2+Z; #3 1/2+X, 1/2-Y, 1/2+Z; #4 1-X, 1-Y, 1-Z.

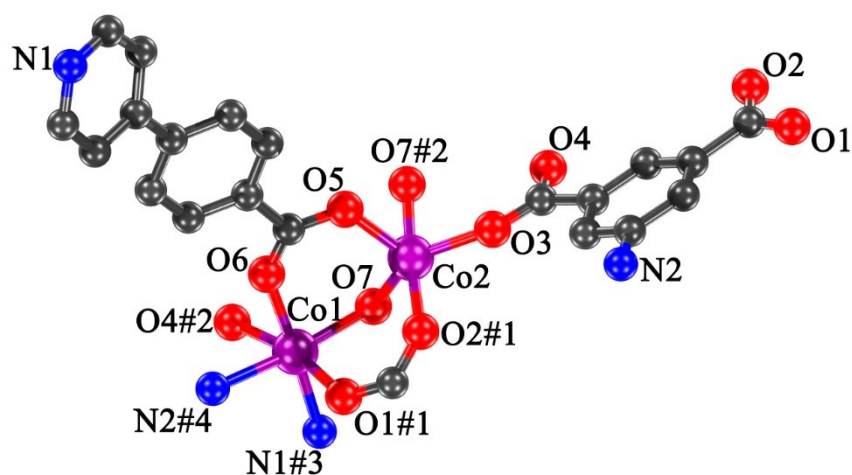


Fig. S1 The coordination environment diagram in **JLNU-500**, symmetry codes: #1 $1/2-X, -1/2+Y, 1/2-Z$; #2 $1-X, 1-Y, 1-Z$; #3 $-1/2+X, 1/2-Y, 1/2+Z$; #4 $1/2+X, 1/2-Y, 1/2+Z$. All hydrogen atoms have been omitted for clarity. Violet = Co; dark gray = C; red = O; blue = N.

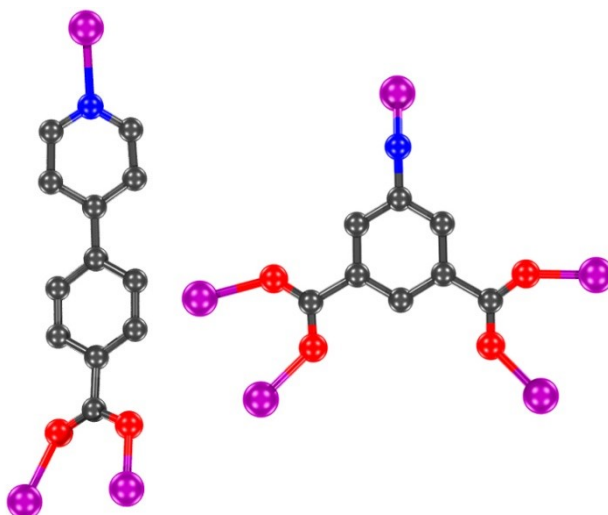


Fig. S2 The coordination modes of ligands in **JLNU-500**.

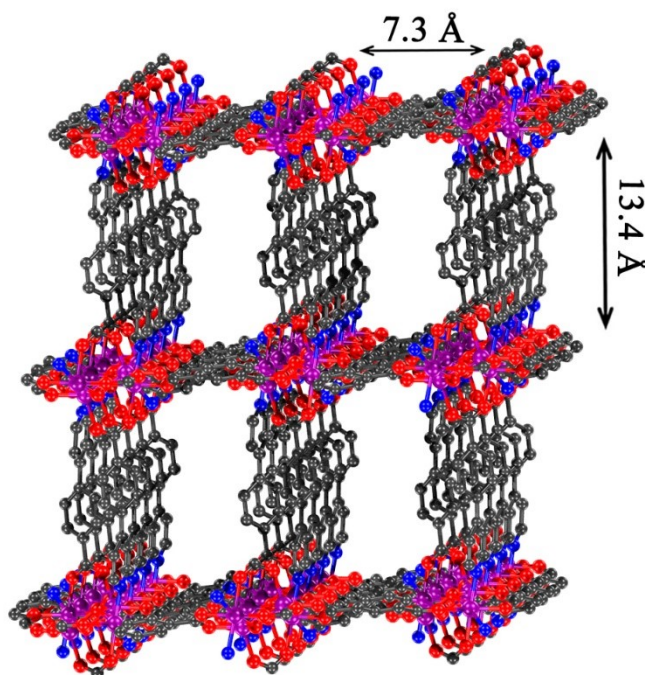


Fig. S3 Ball-and-stick representation of the 3D network of **JLNU-500** viewed from *b* axis and the channel ($13.4 \text{ \AA} \times 7.3 \text{ \AA}$).

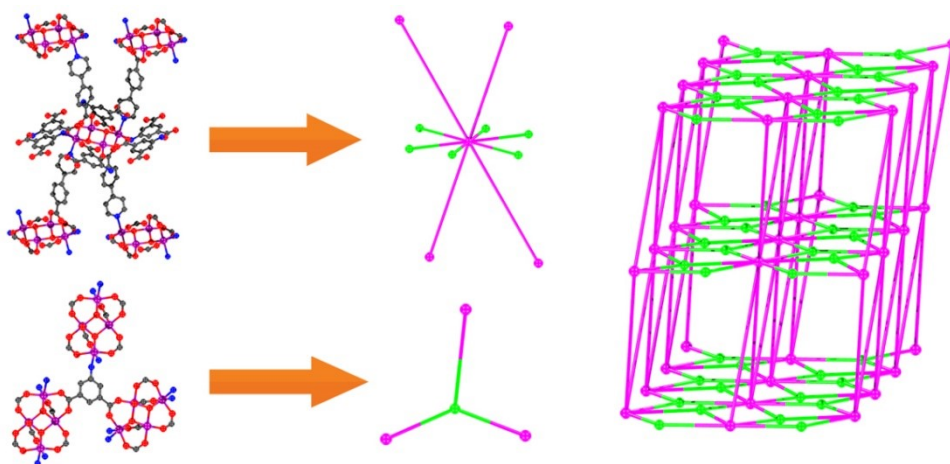


Fig. S4 The (3,10)-connected topology network in **JLNU-500**.

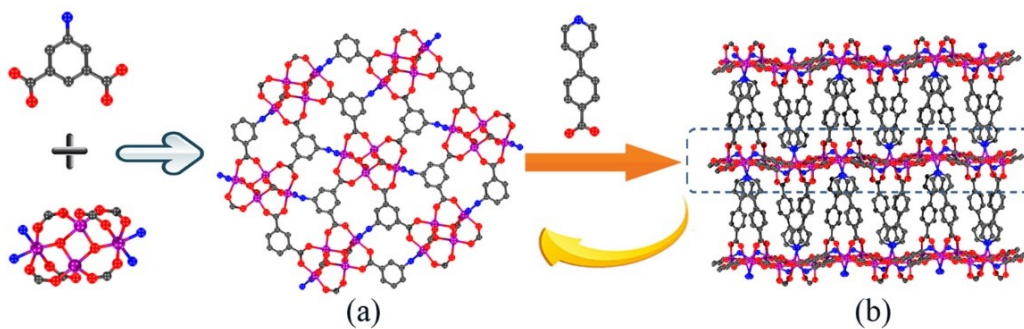


Fig. S5 (a) The layer is formed by Co_4O_2 clusters and AIP^{2-} ligands, (b) ball-and-stick representations of the 3D pillared-layer structure of **JLNU-500**.

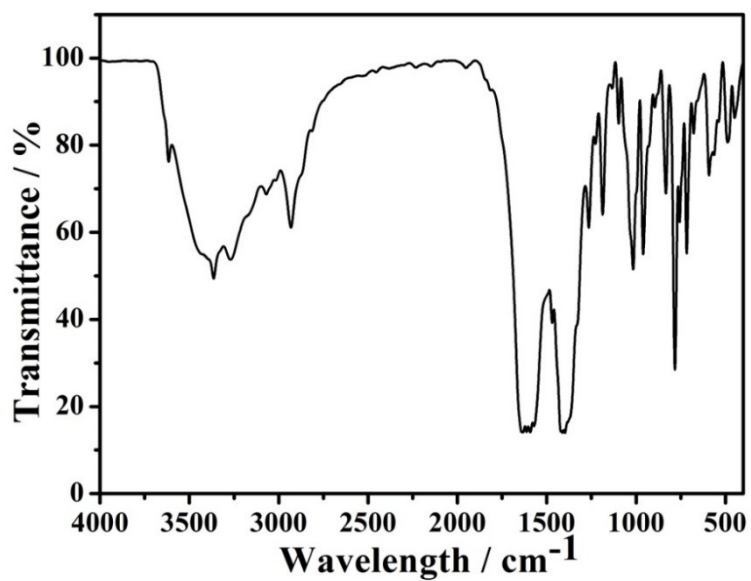


Fig. S6 The FT-IR curve of as-synthesized **JLNU-500** at room temperature.

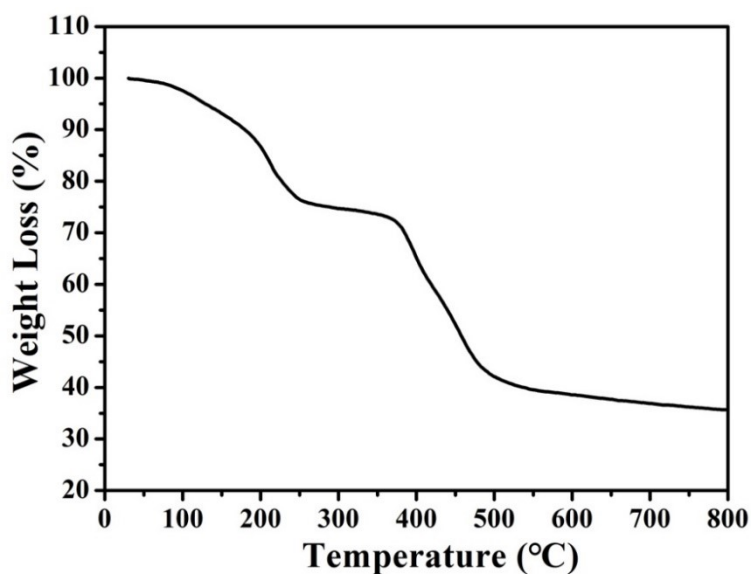


Fig. S7 TGA curve of as-synthesized **JLNU-500** under nitrogen gas atmosphere.

Table S4 Comparison of different Co-containing catalysts towards pollutants for PMS activation.

Catalyst	pollutant	PMS dose	Catalyst dose (g/L)	Degradation efficiency (>95%)	Ref.
HCo ₃ O ₄ /C	BPA, 87.6 μm	325.3 μM	0.1	97%, 4 min	5
Co ₃ O ₄ /N/C	Aniline, 20 ppm	0.15 g/L	0.01	99.4%, 10 min	6
Fe ₃ Co ₇ @C-650	BPA, 20 mg/L	0.2 g/L	0.1	98%, 30 min	7
CoMn ₂ O ₄	SA, 10 mg/L	0.1 g/L	0.05	100%, 30 min	8
Co ₃ O ₄ -palygorskite composites	SMX, 30 μM	0.3 mM	0.125	100%, 3.5 min	9
ZIF-67/PAN	AY, 500 mg/L	0.5 g/L	0.233	95.1%, 10 min	10
Co ₃ O ₄ -MC	OTC, 40 μM	0.5 mM	0.2	100%, 12 min	11
NiCo-LDH/10	RR-120, 0.1 mM	3 mM	0.005	89%, 10 min	12
CuCo-MOF-74	MB, 0.2 mM	2.0 mM	0.05	100%, 30 min	13
Co-BTC	DBP, 0.018 mM	1.62 mM	0.3	90%, 5 min	14
Co-MOF	MO, 20 mg/L	1.0 mM	0.1	98.56%, 4.5 min	15
JLNU-500	RhB, 50 mg/L	1.0 mM	0.1	100%, 6 min	this work

BPA, bisphenol A, SA, sulfanilamide, SMX, sulfamethoxazole, AY, acid yellow, OTC, oxytetracycline, RR-120, Reactive Red-120, MB, methylene blue, DBP, dibutyl phthalate, MO, methyl orange.

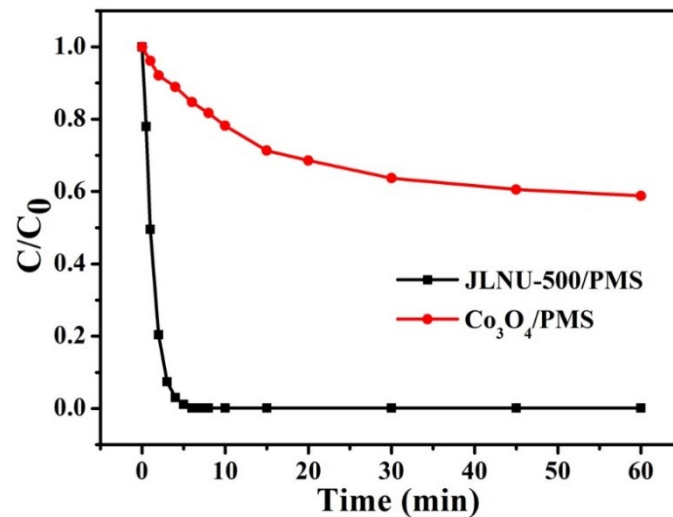


Fig. S8 RhB degradation using **JLNU-500** and Co_3O_4 under the same experimental conditions $[\text{RhB}] = 50 \text{ mg/L}$, $[\text{PMS}] = 1.0 \text{ mM}$, $[\text{JLNU-500}] = 10 \text{ mg}$ or $[\text{Co}_3\text{O}_4] = 10 \text{ mg}$, $T = 20 \text{ }^\circ\text{C}$, initial $\text{pH} = 7.0$.

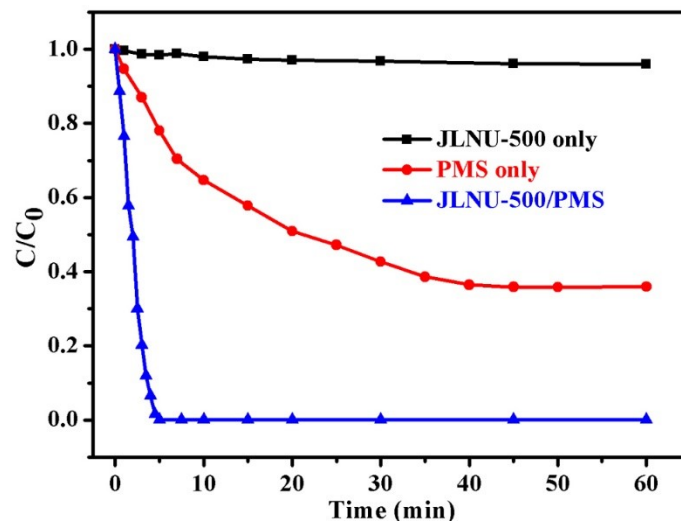


Fig. S9 MO degradation under different reaction conditions $[\text{MO}] = 50 \text{ mg/L}$, $[\text{PMS}] = 1.0 \text{ mM}$, $[\text{JLNU-500}] = 10 \text{ mg}$, $T = 20 \text{ }^\circ\text{C}$, initial $\text{pH} = 7.0$.

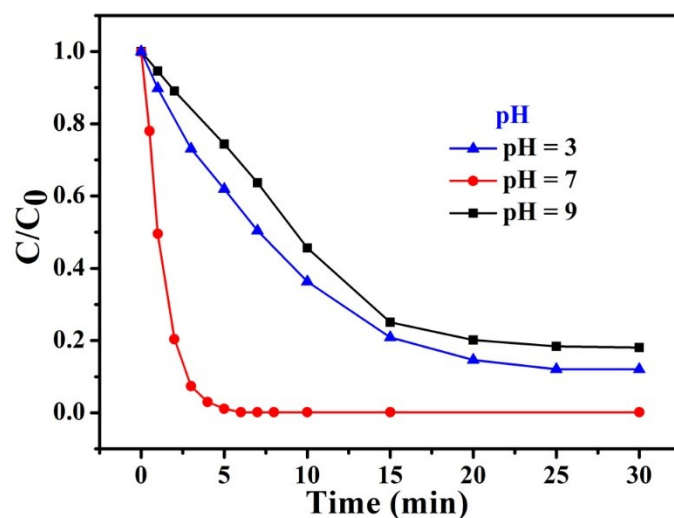


Fig. S10 Effect of pH on the degradation removal of RhB using **JLNU-500/PMS**. [RhB] = 50 mg/L, [PMS] = 1.0 mM; [catalyst **JLNU-500**] = 10 mg; T = 20 °C.

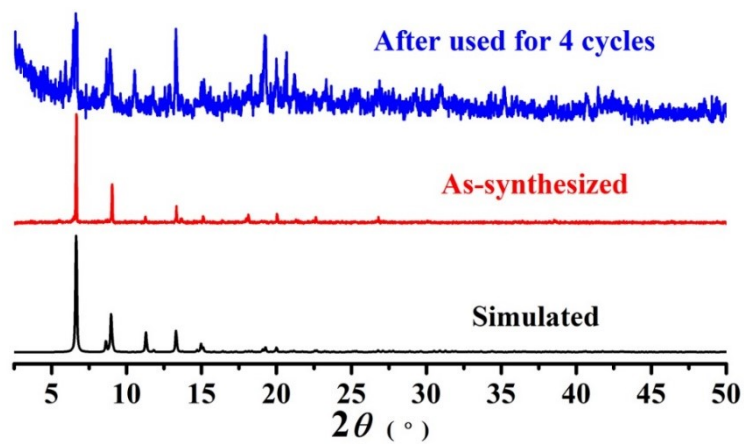


Fig. S11 The PXRD pattern of catalyst **JLNU-500** after being used for 4 cycles.

20230903-xw1a #108-120 RT: 1.15-1.28 AV: 13 SB: 13 0.03-0.16 NL: 4.74E7
T: + c ESI Q1MS [50.000-800.000]

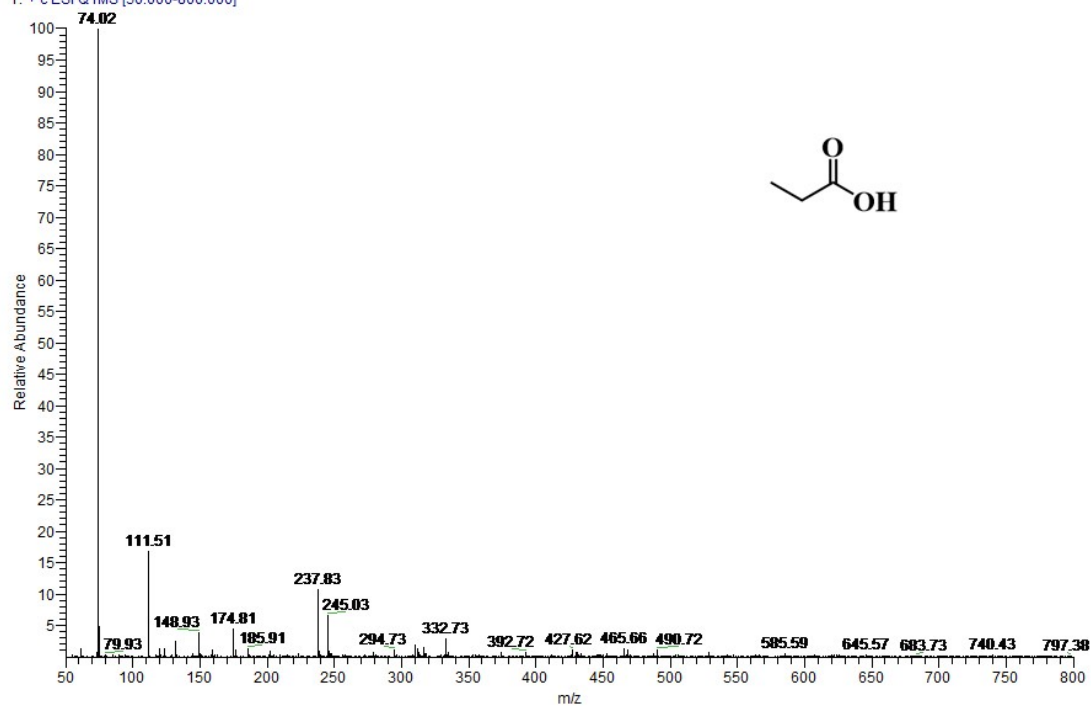


Fig. S12 Mass spectra of 74 in RhB degradation products.

20230903-xw1a #186-208 RT: 1.99-2.22 AV: 23 SB: 13 0.03-0.16 NL: 3.23E8
T: + c ESI Q1MS [50.000-800.000]

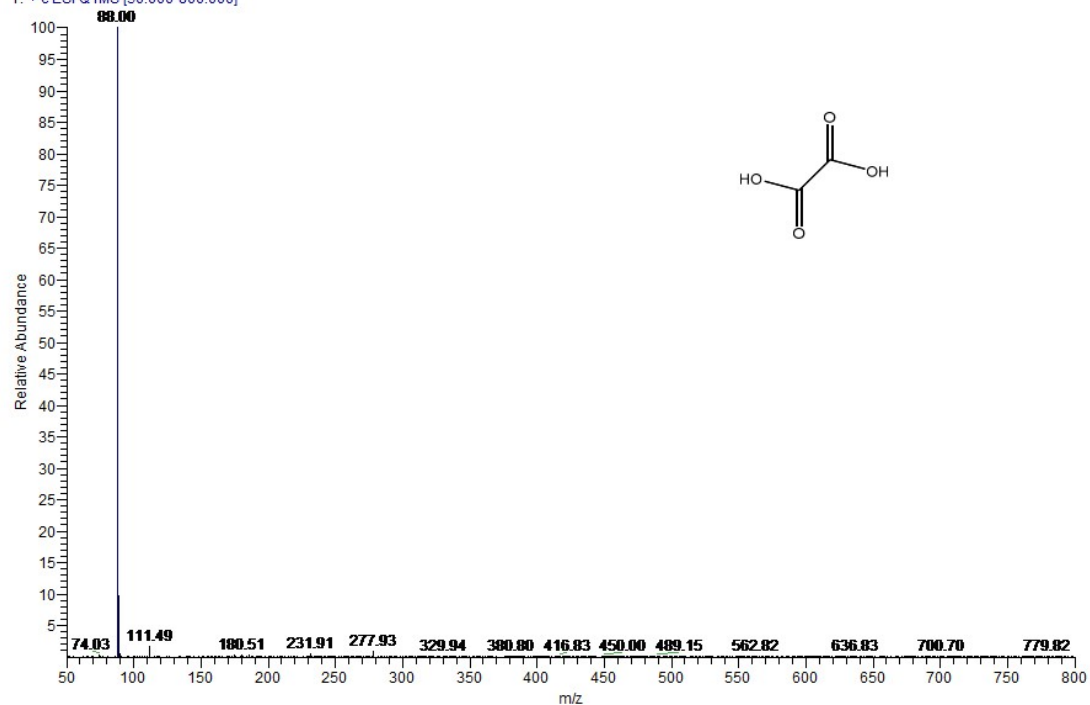


Fig. S13 Mass spectra of 90 in RhB degradation products.

20230903-xw1a#125-153 RT: 1.33-1.63 AV: 29 SB: 13 0.03-0.16 NL: 3.61E7
T: + c ESI Q1MS [50.000-800.000]

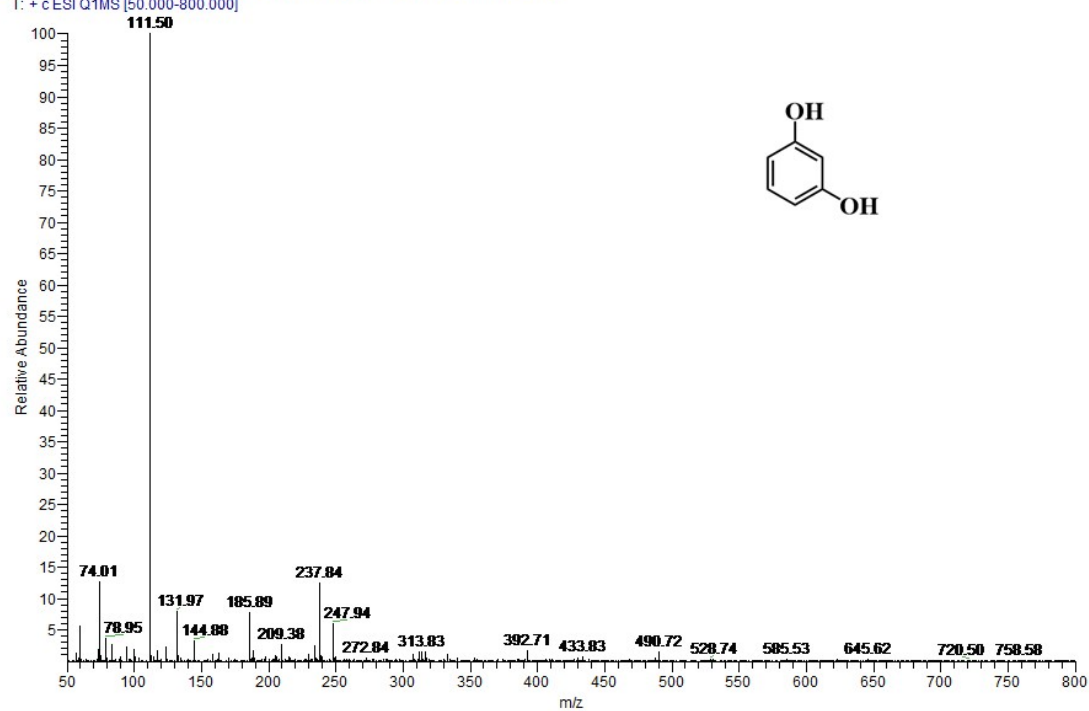


Fig. S14 Mass spectra of 110 in RhB degradation products.

20230903-xw1a#1234-1262 RT: 13.20-13.50 AV: 29 SB: 38 7.65-8.04 NL: 1.28E7
T: + c ESI Q1MS [50.000-800.000]

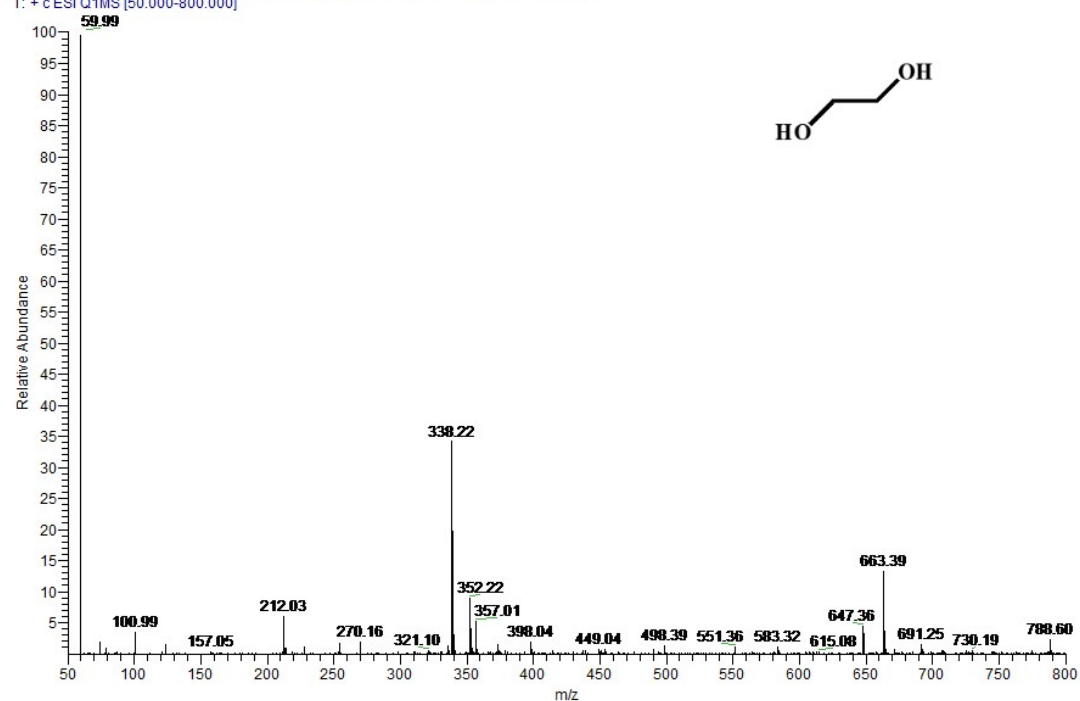


Fig. S15 Mass spectra of 60 in RhB degradation products.

20230903-xw1a #1033-1064 RT: 11.05-11.38 AV: 32 SB: 38 7.65-8.04 NL: 4.13E6
T: + c ESI Q1MS [50.000-800.000]

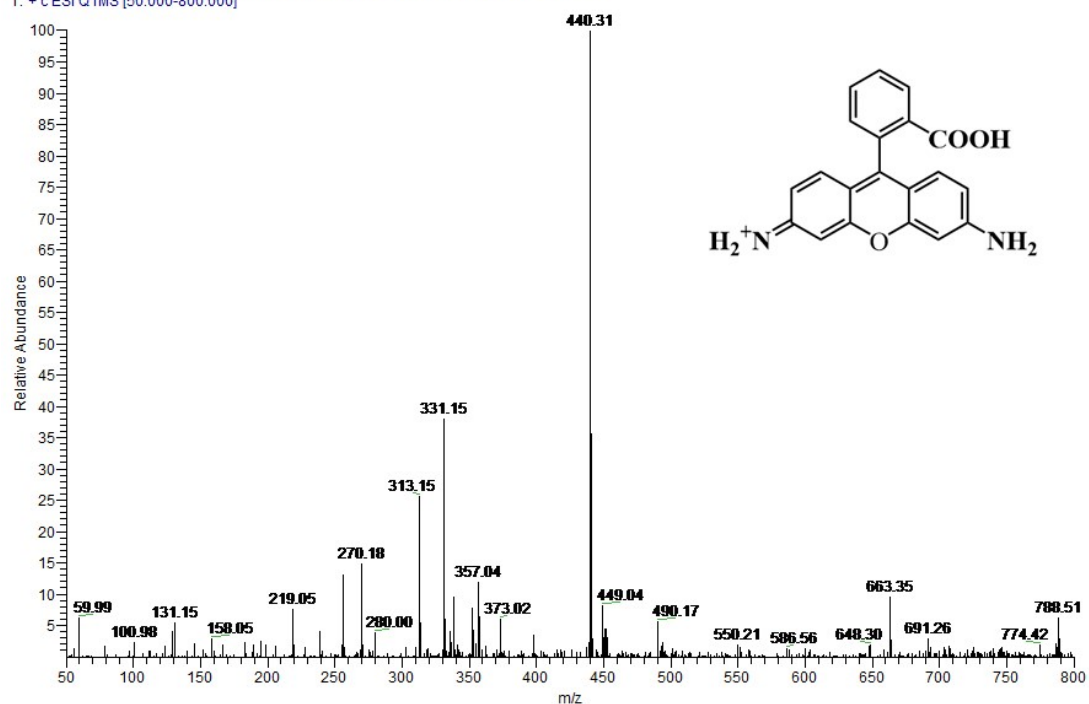


Fig. S16 Mass spectra of 331 in RhB degradation products.

20230903-xw1a #261-285 RT: 2.79-3.05 AV: 25 SB: 13 0.03-0.16 NL: 8.25E7
T: + c ESI Q1MS [50.000-800.000]

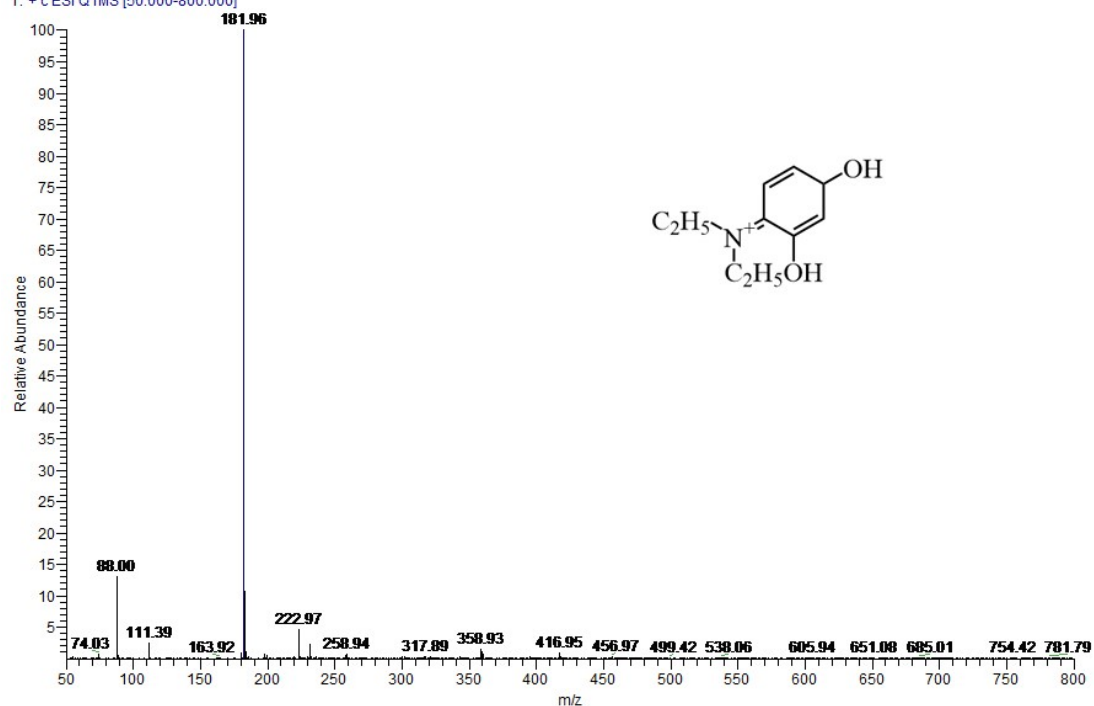


Fig. S17 Mass spectra of 182 in RhB degradation products.

20230903-xw1a #765-790 RT: 8.18-8.45 AV: 26 SB: 38 7.65-8.04 NL: 8.37E6
T: + c ESI Q1MS [50.000-800.000]

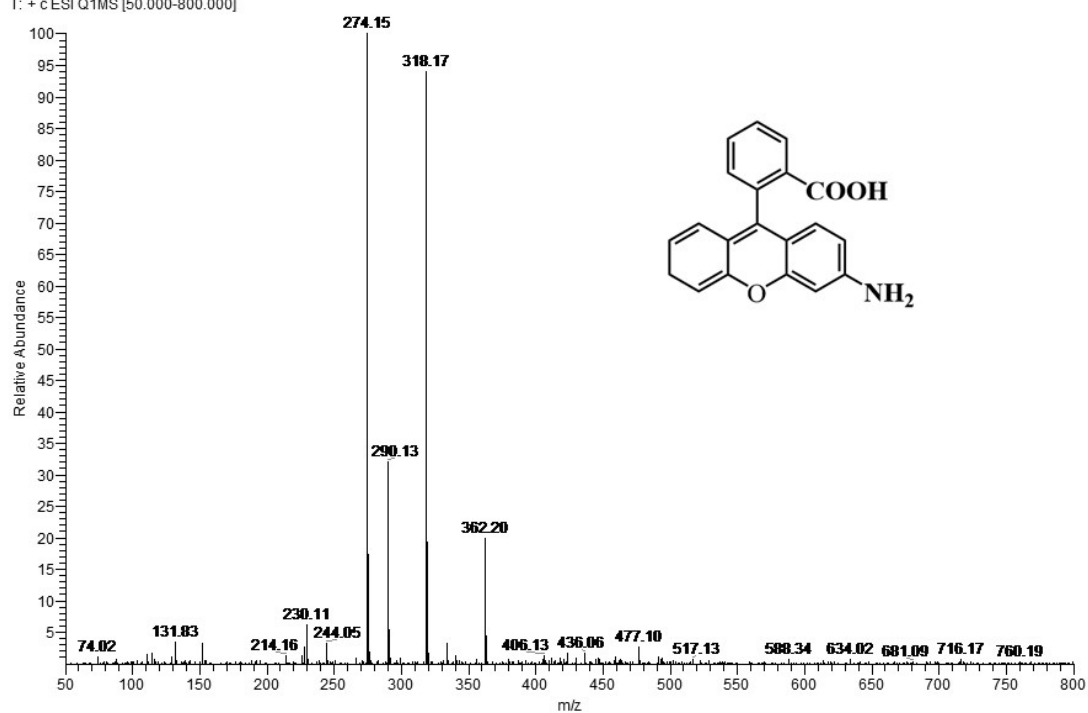


Fig. S18 Mass spectra of 318 in RhB degradation products.

20230903-xw1a #983-994 RT: 10.52-10.63 AV: 12 SB: 38 7.65-8.04 NL: 1.15E7
T: + c ESI Q1MS [50.000-800.000]

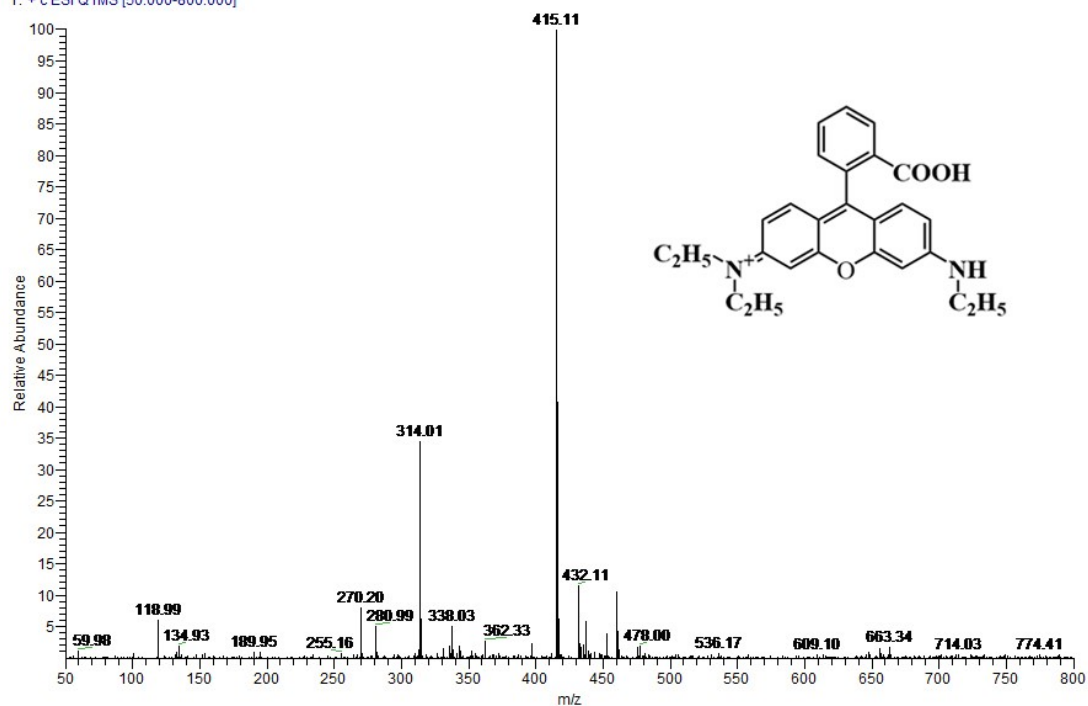


Fig. S19 Mass spectra of 415 in RhB degradation products.

References:

1. L. J. Bourhis, O. V. Dolomanov, R. J. Gildea, J. A. K. Howard, H. Puschmann, *Acta Cryst. A.*, 2015, **71**, 59-75.
2. O. V. Dolomanov, L. J. Bourhis, R. J. Gildea, J. A. K. Howard, H. Puschmann, J. *Appl. Crystallogr.*, 2009, **42**, 339-341.
3. G. M. Sheldrick, *Acta Cryst. C.*, 2015, **71**, 3-8.
4. A. Spek, *Acta Cryst. D.*, 2009, **65**, 148-155.
5. M. A. N. Khan, P. K. Klu, C. Wang, W. Zhang, R. Luo, M. Zhang, J. Qi, X. Sun, L. Wang, J. Li, *Chem. Eng. J.*, 2019, **363**, 234-246.
6. Q. Huang, J. Zhang, Z. He, P. Shi, X. Qin, W. Yao, *Chem. Eng. J.*, 2017, **313**, 1088-1098.
7. X. Li, A. I. Rykov, B. Zhang, Y. Zhang, J. Wang, *Catal. Sci. Technol.*, 2016, **6**, 7486-7494.
8. C.-X. Li, C.-B. Chen, J.-Y. Lu, S. Cui, J. Li, H.-Q. Liu, W.-W. Li, F. Zhang, *Chem. Eng. J.*, 2018, **337**, 101-109.
9. Y. Yu, Y. Ji, J. Lu, X. Yin, Q. Zhou, *Chem. Eng. J.*, 2021, **406**, 126759.
10. C. Wang, H. Wang, R. Luo, C. Liu, J. Li, X. Sun, J. Shen, W. Han, L. Wang, *Chem. Eng. J.*, 2017, **330**, 262-271.
11. Z. Li, M. Wang, C. Jin, J. Kang, J. Liu, H. Yang, Y. Zhang, Q. Pu, Y. Zhao, M. You, Z. Wu, *Chem. Eng. J.*, 2020, **392**, 123789.
12. R. Ramachandran, T. Sakthivel, M. Li, H. Shan, Z.-X. Xu, F. Wang, *Chemosphere*, 2021, **271**, 128509.
13. H. Li, Z. Yang, S. Lu, L. Su, C. Wang, J. Huang, J. Zhou, J. Tang, M. Huang, *Chemosphere*, 2021, **273**, 129643.
14. H. Li, J. Wan, Y. Ma, Y. Wang, X. Chen, Z. Guan, *J. Hazard. Mater.*, 2016, **318**, 154-163.
15. W. Xie, Y. Yuan, W. Jiang, S.-R. Zhang, G.-J. Xu, Y.-H. Xu, Z.-M. Su, *CrystEngComm*, 2022, **24**, 6786-6792.